

# Observing single biomolecules at work with the atomic force microscope

Andreas Engel<sup>1</sup> and Daniel J. Müller<sup>1,2</sup>

**Progress in the application of the atomic force microscope (AFM) to imaging and manipulating biomolecules is the result of improved instrumentation, sample preparation methods and image acquisition conditions. Biological membranes can be imaged in their native state at a lateral resolution of 0.5–1 nm and a vertical resolution of 0.1–0.2 nm. Conformational changes that are related to functions can be resolved to a similar resolution, complementing atomic structure data acquired by other methods. The unique capability of the AFM to directly observe single proteins in their native environments provides insights into the interactions of proteins that form functional assemblies. In addition, single molecule force spectroscopy combined with single molecule imaging provides unprecedented possibilities for analyzing intramolecular and intermolecular forces. This review discusses recent examples that illustrate the power of AFM.**

To observe biomolecules at work they must reside in their native environments. For soluble proteins this is a physiological buffer. Membrane proteins, in addition, need to be embedded in a lipid bilayer. The only instrument that can image samples at sub-nanometer resolutions and be operated in solution is the atomic force microscope (AFM)<sup>1</sup>. This instrument uses a sharp stylus at the end of a flexible cantilever to scan over the sample surface. Cantilever deflections measured at a resolution of a few angstroms are used to determine the surface contour of the sample, exploiting a sensitive feedback to minimize the force applied to the stylus. Recent progress in the field is the result of the optimization of sample preparation<sup>2–5</sup> and image acquisition<sup>6,7</sup> methods, and continuous developments in the instrumentation<sup>8–10</sup>.

Images showing the surface topography — topographs — of biomolecules are attractive not only because they reveal the object in its native state, but also because they exhibit an outstanding signal-to-noise (S/N) ratio. Striking images have been recorded that show submolecular features of single biomolecules (Fig. 1). Minute structural changes at the surfaces of biomolecules can be detected with a time resolution of a few milliseconds, sufficient to monitor conformational changes involved in biological processes. Finally, the AFM stylus is a nanotool that can manipulate single molecules.

## High resolution imaging

Biomolecular forces lie between a few piconewtons (pN), as generated, for example, by myosin, and 300 pN, the force required to unfold a protein<sup>11–13</sup>. It is important to ensure that imaging forces between the stylus and sample are generally of similar magnitudes, because higher forces would lead to sample distortion or even destruction. Electrostatic and van der Waals interactions are the major forces between the AFM stylus and biological samples for imaging in a buffer solution<sup>14,15</sup>. Force-distance curves, which are acquired by approaching the sample with the stylus while measuring its deflection, reveal the nature of these forces<sup>16,17</sup>. These forces can be minimized by adjusting the electrolyte concentration and pH of the buffer<sup>6</sup>. In addition, AFM feedback parameters must be optimized to ensure distortion-

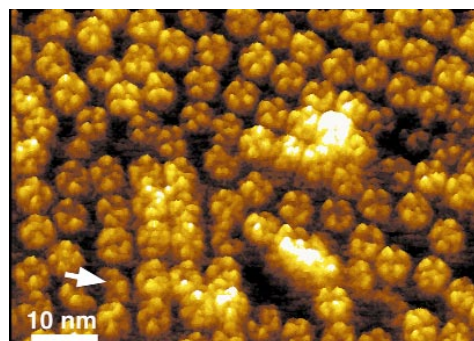


**Fig. 1** Surface topograph of the major intrinsic proteins (MIP) from lens fiber cells recorded in buffer<sup>22</sup>. The MIP tetramers form highly ordered tetragonal, double-layered arrays by reconstitution into a lipid bilayer. To reveal the lower layer, the upper layer was removed with the AFM stylus, thereby disrupting the crystal order and occasionally the tetramers (arrow). The topograph exhibits a vertical range of 1.6 nm. All topographs shown here and in Figs 2,4,5 are displayed as a relief tilted by 5°.

free imaging<sup>7</sup>. After such adjustments, topographs of protein surfaces revealing details with a lateral resolution of 0.5 nm and a vertical resolution of 0.1 nm can be recorded routinely<sup>18–22</sup>.

A quantitative comparison of topographs and structural data obtained by electron and X-ray crystallography of bacteriorhodopsin (BR), the light driven proton pump that is packed in regular arrays in the plasma membrane of *Halobacterium salinarum*, demonstrates the accuracy of data recorded by AFM<sup>23</sup>. Images of individual BR trimers within such arrays allow the precision of AFM topographs to be evaluated by comparing average and standard deviation (SD) maps (Fig. 2a) with the atomic structures. Surface contours of BR defined by the average fit to the atomic structure within the SD (typically 0.1 nm). In addition, SD maps of BR correlate very well with the root mean square (r.m.s.) deviation between the atomic models derived from X-ray and electron crystallography (Fig. 2b). Thus, the AFM provides topographs that allow the determination not only of height and location but also the dynamics of loops connecting

<sup>1</sup>M.E. Müller Institute for Structural Biology, Biozentrum, CH-4056 Basel, Switzerland. <sup>2</sup>Max-Planck-Institute of Molecular Cell Biology and Genetics, D-01307 Dresden, Germany.

Correspondence should be addressed to A.E. email: [andreas.engel@unibas.ch](mailto:andreas.engel@unibas.ch)

## review

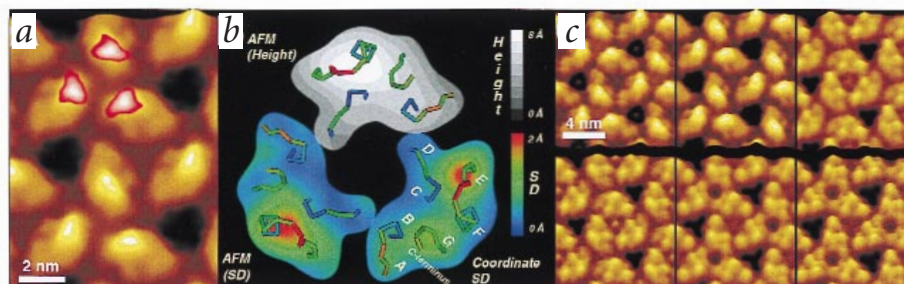


**Fig. 2** Quantitative analyses of the native cytoplasmic purple membrane surface. **a**, Correlation average of the AFM topograph recorded at an applied force of 100 pN (ref. 19). Regions with enhanced flexibility are derived from SD maps and superimposed in red to white shades. **b**, Different surface properties of bacteriorhodopsin (BR). The surface loops are shown as backbone tracings colored according to the backbone r.m.s. deviation (SD) calculated after superimposing five different atomic models of BR<sup>23</sup>. The gray scale image shows the height map determined by AFM (**a**) with the prominent protrusion representing the EF loop. The colored monomers represent the coordinate SD between the atomic models, and the SD of the height measured by AFM. **c**, Unraveling the force induced structural changes of the cytoplasmic surface by multivariate statistical analysis. Top left: purple membrane imaged at 80 pN. Top center: the same membrane imaged at ~100 pN. Top right: at ~150 pN the EF loop is bent away while the shorter polypeptide loops of the cytoplasmic surface become visible. Bottom row: three conformations of BR trimers that differ in their central protrusion are observed at ~180 pN. The topographs exhibit a vertical range of 1 nm.

transmembrane secondary structures. Moreover, classification of single molecule images by multivariate statistical analysis reveals their conformational states (Fig. 2c).

Recent examples illustrate the power of the AFM to image native membrane protein surfaces. The AFM is sufficiently sensitive to detect changes introduced by proteolysis. Topographs of bacterial water channels, AqpZ<sup>20</sup>, and animal eye lens water channels, MIP<sup>22</sup>, recorded before and after proteolytic digestion allowed the cytoplasmic side to be identified. Topographs of a BR-rhodopsin chimera gave well-defined boundary conditions for building a model of the functionally important EF loop of rhodopsin grafted onto BR<sup>24</sup>. Images of the reconstituted cylindrical complex assembled from subunit III of the chloroplast F<sub>0</sub>F<sub>1</sub>-ATP synthase provided compelling evidence that the membrane resident F<sub>0</sub> complex comprises a ring of 14 subunits<sup>21</sup>. This finding is in contrast to the stoichiometry of the *Escherichia coli* F<sub>0</sub> complex that was postulated to comprise a dodecamer of subunit c. This postulation was based mainly on crosslinking experiments<sup>25</sup>, genetic engineering<sup>26</sup>, model building<sup>27–29</sup> and the fact that four protons are required to traverse this molecular motor for the synthesis of one ATP. Interestingly, X-ray analyses of entire yeast F<sub>0</sub>F<sub>1</sub>-ATP synthase crystals revealed the F<sub>0</sub> part to contain a decameric ring<sup>30</sup>, indicating that polymorphic stoichiometries of F<sub>0</sub> complexes may have a biological origin that is not yet understood. While X-ray crystallography showed  $\alpha$ -hemolysin to assemble into heptameric channels<sup>31</sup>, topographs of native  $\alpha$ -hemolysin integrated in a supported bilayer demonstrate that a hexameric form exists as well<sup>4</sup>.

For technical applications, AFM has been used to monitor the growth of two-dimensional crystals of annexin V on a supported lipid bilayer<sup>32</sup> as well as the growth of three-dimensional crystals of various soluble proteins in natural mother liquor, thereby revealing the origin of crystal defects<sup>33</sup>.

### Observing single molecules at work

Because topographs are recorded in buffer solution, an exciting possibility is that single molecules may be observed at work. A major obstacle to achieving this goal is the possible inactivation of the biological process upon immobilizing the sample on a flat support, which is required for contact mode imaging. Since tapping mode AFM minimizes lateral forces, weakly adsorbed single molecules may be imaged at sufficient resolution to monitor enzyme activity. The experimental conditions can thus be adjusted to switch the biological process on or off at will by simply changing

the buffer. A breakthrough demonstrating these possibilities was the direct observation of RNA polymerase activity by time-lapse tapping mode AFM (Fig. 3)<sup>34</sup>. This approach also allowed recording of the one-dimensional diffusion of RNA polymerase along DNA, with and without transcription<sup>35</sup>. In another example, time-lapse series of amyloid fibers adsorbed onto mica were recorded to monitor their growth<sup>36</sup>. To improve the time resolution, the tapping frequencies of the AFM need to be increased. The recent development of small cantilever AFM<sup>10</sup> is an excellent approach to achieving higher tapping frequencies, as demonstrated with the direct visualization of the binding and dissociation of GroES to GroEL that is tethered to mica by electrostatic forces<sup>37</sup>. The GroE system is the bacterial chaperonin that assist protein folding inside the cells. This example thus demonstrates that protein folding at the single molecule level may be monitored in the future.

### Conformational changes of membrane channels

Immobilization of two-dimensional assemblies requires small forces that do not interfere with their biological functions, for example those of the hexagonally packed intermediate (HPI) layer. This regular protein layer that is an integral constituent of the cell envelope of *Deinococcus radiodurans* and is probably involved in protection and stabilization of underlying cell structures. It is assembled from hexameric units comprising a core with a central channel and six spokes that connect to adjacent hexamers. Two conformations of the hexagonally packed intermediate layer have been identified<sup>38</sup>. The central pore appears to exist in a plugged and an unplugged conformation that interchange randomly from one scan to the next (Fig. 4a,c). This observation suggests that the HPI layer could serve as molecular sieve with an open and a closed state, supporting its putative protecting function.

The structurally and functionally well-characterized porin OmpF, a trimeric membrane channel, is a major outer membrane protein of *E. coli*. It consists of 16 antiparallel  $\beta$ -strands that line the transmembrane pore<sup>39</sup>. The strands are connected by short turns at the periplasmic side of the membrane (Fig. 5a) and long loops at the extracellular surface, which form a domain that protrudes up to 1.3 nm above the bilayer (Fig. 5b). Three conditions induce a displacement of this domain towards the trimeric center, which results in a structure with a height of only 0.6 nm above the bilayer<sup>18</sup>: (i) application of an electric potential >200 mV across the membrane; (ii) generation of a K<sup>+</sup> gradient >0.3 M (Fig. 5c); and (iii) acidic pH ( $\leq 3$ ; Fig. 5d). This displacement of the extracellular domain leads to the closure of the channel, suggesting a

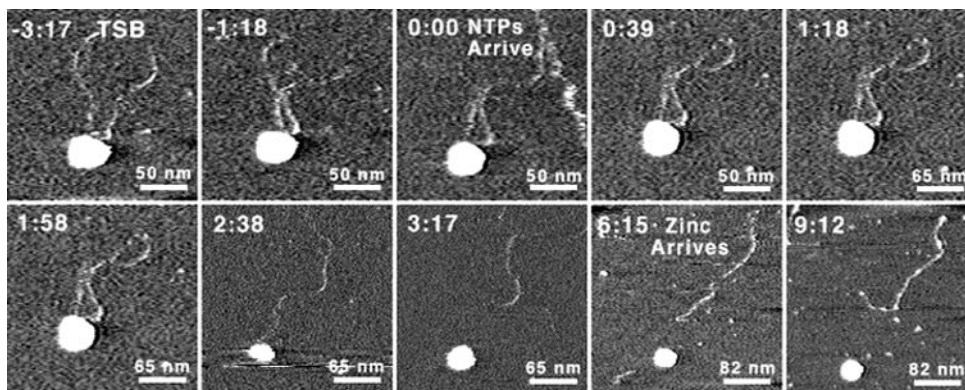


**Fig. 3** RNA polymerase at work<sup>34</sup>. Polymerase–DNA complexes were adsorbed on to mica and washed in transcription buffer (TSB) to facilitate slow diffusion of DNA on mica. A rapid displacement of the DNA with respect to the RNA polymerase is observed after addition of the nucleotides (NTP). High resolution imaging was possible after addition of Zn<sup>2+</sup>, which immobilizes DNA on the support. The time is indicated in minutes.

protective role at low pH — *E. coli* cells passing through the acidic milieu of a stomach may survive longer by closing the outer membrane pores. The first condition, however, is compatible with results from electrophysiological experiments that demonstrated that porin is a voltage gated channel<sup>40</sup>.

### Manipulation of single molecules

Considering the resolutions attainable with AFMs, it is possible that the stylus could be used as a molecular scalpel. This was first demonstrated with single DNA molecules<sup>41</sup> and subsequently by the splitting of gap junctions, double layered two-dimensional arrays of cell-to-cell channels<sup>42</sup>. Splitting of regular double layers with the stylus was also achieved with porin *OmpF*<sup>43</sup> as well as with the eye lens water channel *MIP*<sup>22</sup>. In all cases, the splitting allowed high resolution imaging of the buried surface beneath the top layer. In a different type of molecular manipulation, chromosomes have been dissected and the DNA fragments adsorbed onto the stylus tip subsequently amplified by PCR, providing a means to identify the location of a specific sequence on a particular region of the chromosome<sup>44</sup>. The stylus even allows single protein complexes to be dissected, as demonstrated by the mechanical disassembly of photosystem I complexes, thereby revealing the interface between the membrane resident proteins and the extrinsic proteins<sup>45</sup>. These examples illustrate the variety of molecular ‘surgery’ made possible with the AFM stylus.

Even without imaging, a wealth of information on the unfolding of proteins and the nature of molecular interactions has been

collected by recording force extension curves<sup>12</sup> (see the review by Fernandez and coworkers<sup>46</sup>, in this issue). We have demonstrated the possibility of extracting a single protein from a supramolecular structure and identifying the resulting vacancy produced by recording a high resolution topograph after the unzipping event (Fig. 4). While initial experiments performed with the HPI layer<sup>47</sup> revealed that the spokes connecting adjacent hexamers were the weakest packing interactions, force extension curves acquired with purple membrane could be interpreted to greater detail based on the atomic structure of BR. In the latter case, it was observed that the transmembrane  $\alpha$ -helices unfold by two different pathways<sup>13</sup>. Combining single molecule force spectroscopy and imaging opens an avenue for assessing the forces driving the assembly of supramolecular structures at the level of single molecules.

### Perspectives

Images and force extension curves acquired with the AFM by other groups<sup>2,4,8,9,11,12,37,46,48</sup> and the examples discussed here demonstrate the power of this instrument for studying the structures, functions and dynamics of biomolecules. Both the high resolution and outstanding S/N ratios provided by the AFM allow such analyses to be achieved with single molecules. To study their dynamics, small cantilevers now allow real time measurements at scanning rates of 20 Hz or faster<sup>10</sup>. What developments and novel applications might we expect in the future? A few selected examples may give some hints about the future of biological AFM.

With respect to instrumentation, higher sensitivities and faster feedback will complement the development of small cantilevers

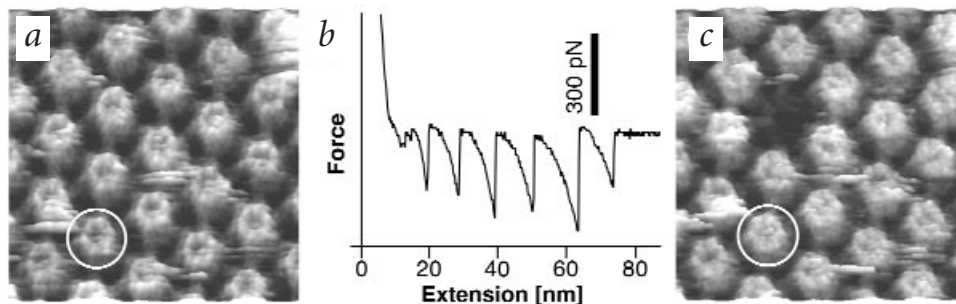


**Fig. 4** Conformational change and single molecule force spectroscopy of the HPI layer<sup>38,47</sup>. **a**, Inner surface of the HPI layer showing hexameric pores. Individual pores exist in plugged or unplugged conformations. **b**, After taking the image the AFM stylus was pushed onto the HPI surface and retracted. Occasionally, the force extension curve recorded showed a sawtooth like pattern with up to six force peaks of ~300 pN each. **c**, The same surface area imaged after recording the force extension curve shows that an entire hexameric pore was removed. The emanating arms of the adjacent pores to which the unzipped hexamer was connected are clearly visible. A few individual pores have changed their conformations between recording the first and the second topographs (circled). This conformational change is fully reversible and can be observed over hours. The topographs exhibit a vertical range of 3 nm, while the center-to-center distance between hexamers is 18 nm.

## review

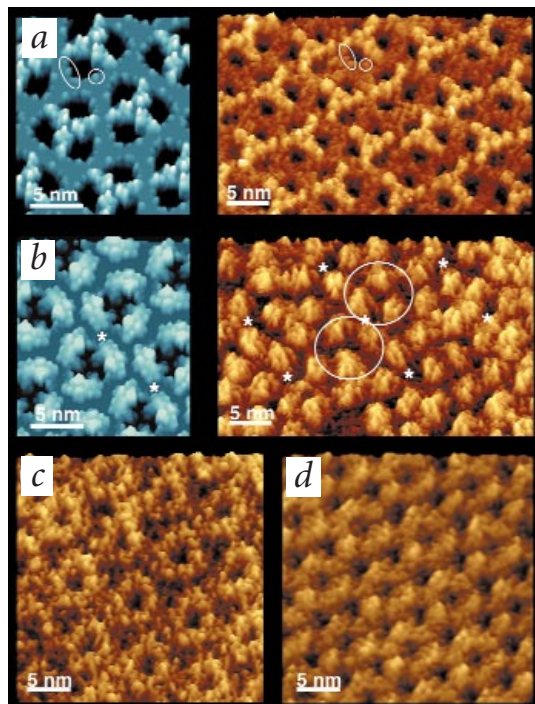


**Fig. 5** Conformational changes of porin OmpF<sup>18</sup>. **a**, The atomic model of the periplasmic surface rendered at 0.3 nm resolution (left) exhibits features that are recognized in the unprocessed topograph (right). Short  $\beta$ -turns comprising only a few amino acids are sometimes distinct (oval and circle). **b**, The extracellular surface of OmpF. The comparison between the atomic model (left) and the topograph (right) illustrates that the loops that protrude 1.3 nm from the bilayer are flexible. The asterisks mark the twofold symmetry axis of the rectangular unit cells housing two porin trimers. **c**, pH dependent conformational change of the extracellular surface. At pH  $\leq 3$  the flexible loops reversibly collapse towards the center of the trimer thereby reducing their height to 0.6 nm. **d**, Conformational change of porin induced by an electrolyte gradient. The monovalent electrolyte gradient across the membrane was  $>300$  mM. Similar to the pH dependent conformational change, the extracellular domains reversibly collapsed onto the porin surface. The topographs exhibit a vertical range of (a) 1 nm (b) 1.5 nm, and (c,d) 1.2 nm.

to further increase scanning speeds while reducing the forces between the stylus and samples. Multifunctional cantilevers such as those currently being developed for other applications<sup>49,50</sup>, such as nanolithography and surface nanochemistry, will provide novel experimental opportunities. A combined optical probe/AFM stylus could photolyse and release caged ATP locally to initiate biological reactions, such as ATP induced motion of molecular motors, while the function-related conformational changes of the biomolecules involved will be observed with the stylus of the AFM. This type of probe may also be of interest for observing supramolecular assemblies that include fusion constructs comprising a green fluorescent protein. A combined scanning micropipette/AFM stylus could deposit ligands locally while the stylus monitors the binding process. Electric stimuli could be applied to a single voltage-gated channel with an electrically insulated probe that may include the micropipette/AFM stylus, allowing the opening or closing of the channel to be observed directly.

As the functionality of AFMs improve, it might become possible to study native structures within a complex molecular assembly, in which different protein subunits interact with one another to form the functional machinery. Techniques that involve averaging processes to eliminate noise do not allow single proteins to be studied within such structures. In contrast, the AFM opens an

exciting new avenue for assessing the interaction between single proteins in such supramolecular complexes. While unzipping single molecules *in vitro* and dissecting supramolecular structures now provide information on the intermolecular and intramolecular forces involved, sensing and imaging capabilities of future instruments will allow similar measurements to be performed with organelles and living cells. Such experiments will give new information about cellular trafficking and interactions. The potential of the AFM to monitor multiple signals and to manipulate processes at the cell surface could be extended by combining AFM with optical microscopy. These instruments will be important for gaining a deeper understanding of cellular networks.

#### Acknowledgments

We gratefully thank D. Fotiadis for Fig. 1 and H. Hansma for the time-lapse series shown in Fig. 3. This work was supported by the Maurice E. Müller Foundation of Switzerland, and the Swiss National Foundation for Scientific Research.

Received 23 June, 2000; accepted 1 August, 2000.

- Binnig, G., Quate, C.F. & Gerber, C. *Phys. Rev. Lett.* **56**, 930–933 (1986).
- Mou, J.X., Yang, J. & Shao, Z.F. *J. Mol. Biol.* **248**, 507–512 (1995).
- Müller, D.J., Amrein, M. & Engel, A. *J. Struct. Biol.* **119**, 172–188 (1997).
- Czajkowsky, D.M., Sheng, S. & Shao, Z. *J. Mol. Biol.* **276**, 325–330 (1998).
- Scheuring, S., Müller, D.J., Ringler, P., Heymann, J.B. & Engel, A. *J. Microsc.* **193**, 28–35 (1999).
- Müller, D.J., Fotiadis, D., Scheuring, S., Müller, S.A. & Engel, A. *Biophys. J.* **76**, 1101–1111 (1999).
- Möller, C., Allen, M., Elings, V., Engel, A. & Müller, D.J. *Biophys. J.* **77**, 1050–1058 (1999).
- Hansma, P.K. *et al. Appl. Phys. Lett.* **64**, 1738–1740 (1994).
- Han, W., Lindsay, S.M., Dlakic, M. & Harrington, R.E. *Nature* **386**, 563 (1997).
- Viani, M.B. *et al. J. Appl. Phys.* **86**, 2258–2262 (1999).
- Rief, M., Gautel, M., Oesterhelt, F., Fernandez, J.M. & Gaub, H.E. *Science* **276**, 1109–1112 (1997).
- Fisher, T.E., Oberhauser, A.F., Carrion-Vazquez, M., Marszalek, P.E. & Fernandez, J.M. *Trends Biochem. Sci.* **24**, 379–384 (1999).
- Oesterhelt, F. *et al. Science* **288**, 143–146 (2000).
- Müller, D.J. & Engel, A. *Biophys. J.* **73**, 1633–1644 (1997).
- Rotsch, C. & Radmacher, M. *Langmuir* **13**, 2825–2832 (1997).
- Butt, H.-J., Jaschke, M. & Ducker, W. *Bioelect. Bioenerg.* **38**, 191–201 (1995).
- Heinz, W.F. & Hoh, J.H. *Nanotechnology* **17**, 143–150 (1999).
- Müller, D.J. & Engel, A. *J. Mol. Biol.* **285**, 1347–1351 (1999).
- Müller, D.J., Sass, H.-J., Müller, S., Büldt, G. & Engel, A. *J. Mol. Biol.* **285**, 1903–1909 (1999).
- Scheuring, S. *et al. EMBO J.* **18**, 4981–4987 (1999).
- Seelert, H. *et al. Nature* **405**, 418–419 (2000).
- Fotiadis, D. *et al. J. Mol. Biol.* **300**, 779–789 (2000).
- Heymann, J.B. *et al. J. Struct. Biol.* **128**, 243–249 (1999).
- Heymann, J.B. *et al. Structure Folding Des.* **8**, 643–653 (2000).
- Jones, P.C., Jiang, W. & Fillingame, R.H. *J. Biol. Chem.* **273**, 17178–17185 (1998).
- Jones, P.C. & Fillingame, R.H. *J. Biol. Chem.* **273**, 29701–29705 (1998).
- Groth, G. & Walker, J.E. *FEBS Lett.* **410**, 117–123 (1997).
- Dmitriev, O.Y., Jones, P.C. & Fillingame, R.H. *Proc. Natl. Acad. Sci. USA* **96**, 7785–7790 (1999).
- Rastogi, V.K. & Girvin, M.E. *Nature* **402**, 263–268 (1999).
- Stock, D., Leslie, A.G. & Walker, J.E. *Science* **286**, 1700–1705 (1999).
- Song, L. *et al. Science* **274**, 1859–1866 (1996).
- Reviakine, I., Bergsma-Schutter, W. & Brisson, A. *J. Struct. Biol.* **121**, 356–361 (1998).
- Malkin, A.J., Kuznetsov, Y.G. & McPherson, A. *J. Struct. Biol.* **117**, 124–137 (1996).
- Kasas, S. *et al. Biochem.* **36**, 461–468 (1997).
- Guthold, M. *et al. Biophys. J.* **77**, 2284–2294 (1999).
- Goldsbury, C., Kistler, J., Aebi, U., Arvinte, T. & Cooper, G.J.S. *J. Mol. Biol.* **285**, 33–39 (1999).
- Viani, M.B. *et al. Nature Struct. Biol.* **7**, 644–647 (2000).
- Müller, D.J., Baumeister, W. & Engel, A. *J. Bacteriol.* **178**, 3025–3030 (1996).
- Cowan, S.W. *et al. Nature* **358**, 727–733 (1992).
- Klebba, P.E. & Newton, S.M. *Curr. Opin. Microbiol.* **1**, 238–247 (1998).
- Hansma, H.G. *et al. Science* **256**, 1180–1184 (1992).
- Hoh, J.H., Sosinsky, G.E., Revel, J.-P. & Hansma, P.K. *Biophys. J.* **65**, 149–163 (1993).
- Schäbert, F.A., Henn, C. & Engel, A. *Science* **268**, 92–94 (1995).
- Thalhammer, S., Stark, R.W., Müller, S., Wienberg, J. & Heckl, W.M. *J. Struct. Biol.* **119**, 232–237 (1997).
- Fotiadis, D. *et al. J. Mol. Biol.* **283**, 83–94 (1998).
- Fisher, T.E., Marszalek, P.E. & Fernandez, J.M. *Nature Struct. Biol.* **7**, 719–724 (2000).
- Müller, D.J., Baumeister, W. & Engel, A. *Proc. Natl. Acad. Sci. USA* **96**, 13170–13174 (1999).
- Hinterdorfer, P., Baumgartner, W., Gruber, H.J., Schilcher, K. & Schindler, H. *Proc. Natl. Acad. Sci. USA* **93**, 3477–3481 (1996).
- Wong, S.S., Joselevich, E., Woolley, A.T., Cheung, C.L. & Lieber, C.M. *Nature* **394**, 52–55 (1998).
- Schürmann, G., Noell, W., Staufer, U. & de Rooij, N.F. *Ultramicroscopy* **82**, 33–38 (2000).